Sandia National Laboratories

Scientific Analysis/Calculation Administrative Change Notice

Complete only applicable items.

1. Document Number:	ANL-NBS-HS-000056	2. Revision:	00	3. ACN:	01
4. Title:	Analysis of Alcove 8/Niche 3 Flow and Transport Tests				
5. No. of Pages Attached:	31				

6. Approvals:		
Preparer:	H.-H. Liu Print Name and Sign	12-1-06 Date
Checker:	Charles Haukwa Print name and sign	12-01-06 Date
QCS/Lead Lab QA Reviewer:	Stephen Schuerman Print name and sign	12-01-06 Date
Responsible Manager:	Kenneth Rehfeldt Stephanie Kuzio for Print name and sign	12-01-06 Date

7. Affected Pages	8. Description of Change:
ix, xi, 1-1, 1-2, 2-1, 4-2, 6-1, 6-3, 6-3a, 6-4, 6-5, 6-6, 6-8, 6-10, 6-12, 6-13, 6-20, 6-22, 6-27, 6-28, 6-33, 6-38, 6-39, 6-40, 6-44, 7-3, 8-1, 8-3a, 8-5, A-1, A-2	Editorial changes to address DOE comments and provide additional clarification to strengthen existing discussion.

TABLES

Page

ACRONYMS

ACN	administrative change notice
BSC	Bechtel SAIC Company, LLC
DFBA	Difluorobenzoic Acid
DTN	data tracking number
ECRB	Enhanced Characterization of Repository Block
ESF	Exploratory Studies Facility
MINC	multiple interacting continua
NRC	U.S. Nuclear Regulatory Commission
QA	Quality Assurance
TFBA	Trifluorobenzoic Acid
Tptpmn	Topopah Spring Tuff middle nonlithophysal zone
Tptpul	Topopah Spring Tuff upper lithophysal zone
TSw	Topopah Spring welded hydrogeologic unit
TWP	technical work plan
UZ	unsaturated zone
YMRP	*Yucca Mountain Review Plan, Final Report*

1. PURPOSE

The purpose of this report is to document analyses of the Alcove 8/Niche 3 flow and transport tests, with a focus on the large-infiltration-plot tests and compare pre-test model predictions with the actual test observations. The importance of this analysis is to evaluate modeling approaches for unsaturated zone radionuclide transport as used in performance assessment. The tests involved infiltration that originated from the floor of Alcove 8 (located in the Enhanced Characterization of Repository Block (ECRB) Cross Drift) and observations of seepage and tracer transport at Niche 3 (located in the Main Drift of the Exploratory Studies Facility (ESF)). The test results are relevant to drift seepage and solute transport in the unsaturated zone (UZ) of Yucca Mountain. The main objective of this analysis was to evaluate the modeling approaches used and the importance of the matrix diffusion process by comparing simulation and actual test observations. The pre-test predictions for the large plot test were found to differ from the observations and the reasons for the differences were documented in this report to partly address CR 6783, which concerns unexpected test results. These unexpected results are discussed and assessed with respect to the current baseline unsaturated zone radionuclide transport model in Sections 6.2.4, 6.3.2, and 6.4.

The information provided in this report for the large-infiltration-plot tests in Alcove 8/Niche 3 addresses the request for additional information related to U.S. Nuclear Regulatory Commission (NRC) Key Technical Issue RT 3.05. The characterization of fracture properties for modeling the Alcove 8/Niche 3 flow, drift seepage, and transport processes includes heterogeneous fracture properties in the fractured rock mass and specific fracture properties for the fault present in the test bed. This treatment of fracture properties provides a response to NRC Key Technical Issue SDS 3.01.

The work presented in this report was conducted under *Technical Work Plan for: Unsaturated Zone Flow, Drift Seepage and Unsaturated Zone Transport Modeling* (BSC 2006 [DIRS 177465], Sections 1, 2.1.2, and 2.2.1). No features, events, or processes are planned to be included or excluded as a result of the analyses performed for this report.

Limitations of this scientific analysis are largely determined by uncertainties involved in conceptually understanding the temporal variability of observed seepage rates and the tracer breakthrough signals observed (especially those tracer breakthrough signals recorded during the infiltration pulse observed immediately following scrubbing of the infiltration plots). Based on experimental observations and test conditions, the most plausible conceptual models are implemented in modeling analyses of the testing data. Discussions of conceptual models, their rationale, and the associated uncertainties are presented in Section 6 of this report.

The technical work plan (BSC 2006 [DIRS 177465]) cites procedures that were in effect at the time the work described in this report was planned and approved. Following the transition of the science work scope from Bechtel SAIC Company, LLC (BSC), to Sandia National Laboratories, new procedures were issued and became effective on or after October 2, 2006. This report has been revised to reflect the change to and compliance with Sandia National Laboratories governing procedures. Prior to October 2, 2006, the governing procedure used for this report was the BSC procedure LP-SIII.9Q-BSC, *Scientific Analyses*. This procedure has been superceded by the Sandia procedure SCI-PRO-005, *Scientific Analyses and Calculations*. A

review of the revised procedure found only minor differences. The only difference requiring action regarding this administrative change notice (ACN) was to identify the importance of the report, as stated in SCI-PRO-005, Attachment 2, under requirements for the Purpose section. A statement regarding the importance of this work has been added to this section.

In addition to the changes noted with regard to the governing procedure for this analysis report (SCI-PRO-005), the following procedures implemented in the course of performing this ACN have changed from those identified in the TWP (BSC 2006 [DIRS 177465]). For this ACN, the Sandia procedures listed in Table 1-1 have been implemented:

Table 1-1. Procedure Cross-Walk for Procedures Implemented in the Current ACN

Procedure/Title	BSC Procedure ID (before transition) Identified in BSC 2006 [DIRS 177465]	Sandia Procedure ID (after transition)
Records Management	AP-17.1Q	DM-PRO-002
Control of the Electronic Management of Information	IT-PRO-0009	IM-PRO-002
Managing Technical Product Inputs	PA-PRO-0301	SCI-PRO-004

Some aspects of the implementation of the procedures in Table 1-1 were performed using the BSC procedures prior to October 2, 2006, but were not revised for the purposes of this ACN. Furthermore, the BSC procedures identified in Table 1-2 were implemented in the report prior to transition, in accordance with the TWP (BSC 2006 [DIRS 177465]), but were not required for the development of the ACN. Therefore, the Sandia procedures identified in Table 1-2 have not been implemented in this ACN. There are no impacts of these procedure changes on this analysis report.

Table 1-2. Procedure Cross-Walk for Procedures Not Implemented in the Current ACN, but Used in the Development of This Analysis Report

Procedure/Title	BSC Procedure ID (before transition) Identified in BSC 2006 [DIRS 177465]	Sandia Procedure ID (after transition)
Submittal and Incorporation of Data to the Technical Data Management System	AP-SIII.3Q	TST-PRO-001
Software Management	IT-PRO-0011	IM-PRO-003
Document Review	PA-PRO-0601	SCI-PRO-003

2. QUALITY ASSURANCE

Development of this report and the supporting analysis activities have been determined to be subject to the Yucca Mountain Project's Quality Assurance (QA) Program, as indicated in *Technical Work Plan for: Unsaturated Zone Flow, Drift Seepage and Unsaturated Zone Transport Modeling* (BSC 2006 [DIRS 177465], Section 8.1). Approved QA procedures identified in the technical work plan (TWP) (BSC 2006 [DIRS 177465], Section 4) have been used to conduct and document the activities described in this report. The report was prepared under LP-SIII.9Q-BSC, *Scientific Analyses.* The TWP also identifies the methods used to control the electronic management of data (BSC 2006 [DIRS 177465], Section 8.4) during the modeling analysis and documentation activities.

This report examines the properties of natural barriers (the Upper and Lower Natural Barriers) that are classified in *Q-List* (BSC 2005 [DIRS 175539]) as "Safety Category" because they are important to waste isolation. The report contributes to the analysis used to support total system performance assessment. The conclusions of this report do not affect the repository design or engineered features important to safety.

observed tracer concentration data are used in the sensitivity analyses to evaluate the importance of the matrix diffusion.

All of the direct input data mentioned above are appropriate for this study, because these data are either observations collected from the test sites (infiltration plots and seepage collection points) or modeling results developed specifically for the Alcove 8/Niche 3 tests.

4.2 CRITERIA

Technical requirements to be satisfied by performance assessment are based on 10 CFR 63.114 [DIRS 173273] ("Requirements for Performance Assessment") and 10 CFR 63.115 [DIRS 173273] ("Requirements for Multiple Barriers"). The acceptance criteria that will be used by the NRC to determine whether the technical requirements have been met are identified in *Yucca Mountain Review Plan, Final Report* (YMRP) (NRC 2003 [DIRS 163274]). The pertinent requirements and acceptance criteria for this report are summarized in Table 4-2.

Table 4-2. Project Requirements and YMRP Acceptance Criteria Applicable to This Report

Requirement	YMRP Acceptance Criteria
10 CFR 63.114(a-c)	Criteria 2 and 3 for *Flow Paths in the Unsaturated Zone* and *Radionuclide Transport in the Unsaturated Zone*[a]

[a] From NRC 2003 [DIRS 163274], Sections 2.2.1.3.6.3 and 2.2.1.3.7.3.

The acceptance criteria identified in Sections 2.2.1.3.6 and 2.2.1.3.7 of the YMRP (NRC 2003 [DIRS 163274]) are included below. In cases where subsidiary criteria are listed in the YMRP for a given criterion, only the subsidiary criteria addressed by this report are listed below. Where a subcriterion includes several components, only some of those components may be addressed. How these components are addressed is summarized in Section 7 of this report.

Acceptance Criteria from Section 2.2.1.3.6, *Flow Paths in the Unsaturated Zone*

Acceptance Criterion 2—Data Are Sufficient for Model Justification:

(1) Hydrological and thermal-hydrological-mechanical-chemical values used in the license application are adequately justified. Adequate descriptions of how the data were used, interpreted, and appropriately synthesized into the parameters are provided.

(2) The data on the geology, hydrology, and geochemistry of the unsaturated zone, are collected using acceptable techniques.

(3) Estimates of deep-percolation flux rates constitute an upper bound, or are based on a technically defensible unsaturated zone flow model that reasonably represents the physical system. The flow model is calibrated, using site-specific hydrologic, geologic, and geochemical data. Deep-percolation flux is estimated, using the appropriate spatial and temporal variability of model parameters, and boundary conditions that consider climate-induced change in soil depths and vegetation.

6. SCIENTIFIC ANALYSIS DISCUSSION

This section documents Alcove 8/Niche 3 flow and transport tests, with a focus on the large-infiltration-plot test results (Section 6.1), pre-test prediction of the late stage of the test (Section 6.2), model analyses of test results (Section 6.3), and uncertainties and relevant issues regarding the model analyses (Section 6.4). A flow and transport test within a fault was also conducted near the large-infiltration-plot test site. The test results have been previously documented in *In Situ Field Testing of Processes* (BSC 2004 [DIRS 170004], Section 6.12.4). A discussion of fault test results and a modeling analysis of the results were presented in *UZ Flow Models and Submodels* (BSC 2004 [DIRS 169861], Section 7.6). The information provided in this report for the large-infiltration-plot tests in Alcove 8/Niche 3 addresses the request for additional information related to NRC Key Technical Issue RT 3.05 and SDS 3.01.

The scientific notebooks (with relevant page numbers) used for the modeling analysis activities described in this report are listed in Table 6-1.

Table 6-1. Scientific Notebooks Used in the Modeling Analyses Documented in This Report

Scientific Notebook ID	Relevant Pages	Citation
SN-LBNL-SCI-246-V1	pp. 19 to 50	Lu 2006 [DIRS 176702]
SN-LBNL-SCI-215-V1	pp.160 to 165	Liu 2006 [DIRS 176703]

6.1 ALCOVE 8/NICHE 3 LARGE-INFILTRATION-PLOT TESTS

This section documents Alcove 8/Niche 3 large-infiltration-plot test results. The large-infiltration-plot study was conducted in the ESF in the Yucca Mountain unsaturated zone. The test bed extends from about 190 m to about 215 m (BSC 2004 [DIRS 170004], Section 6.12; Salve 2005 [DIRS 176336]) below the ground surface of Yucca Mountain (Figure 6.1-1). The upper and lower boundaries of the test bed were accessed through two tunnels, referred to as the Cross Drift and the Main Drift, respectively. Alcove 8 is located within the Topopah Spring Tuff upper lithophysal zone (Tptpul). The Tptpul contains large, naturally occurring cavities called lithophysae that are attributed to gas- and vapor-phase constituents entrapped and redistributed during the initial deposition, compaction, and gas migration out of the Topopah Spring welded hydrogeologic unit (TSw). Niche 3 is located within the Topopah Spring Tuff middle nonlithophysal zone (Tptpmn). There is a vertical distance of about 20 m between the floor of Alcove 8 and the crown of Niche 3. The location of the Tptpul–Tptpmn contact is at about 5-6 m above the crown of Niche 3, and about 14 m below the floor of Alcove 8 (BSC 2004 [DIRS 170004], Section 6.12; Salve 2005 [DIRS 176336]).

6.1.1 Testing Methods

Water was released along a surface of fractured welded tuff over a period of about 25 months, between August 2002 and October 2004, during which spatial and temporal variability in infiltration rates was continuously monitored. In addition to the ponded release of water, subsections of the infiltration zone were also perturbed by interruptions to the supply of water and alterations to the plot surface. Observations from this extended infiltration event, with sporadic disruptions, were then analyzed to elucidate mechanisms that influenced the rate at which water moved through the fractured rock surface.

A 3×4 m^2 infiltration plot is located on the floor of Alcove 8 (Figure 6.1-2). The boundary of the plot is made with steel sheets embedded into the floor. The plot is further divided into 12 square subplots, of similar size (i.e., 1 m^2). Each subplot is connected to a permeameter, designed to maintain the desired height of ponded water (approximately 0.02 m) while continuously monitoring the rate at which water is released into the infiltration plot. To minimize losses through evaporation, each infiltration subplot is covered with a plastic sheet, and the Alcove 8 cavity is isolated from ventilation effects by bulkhead doors.

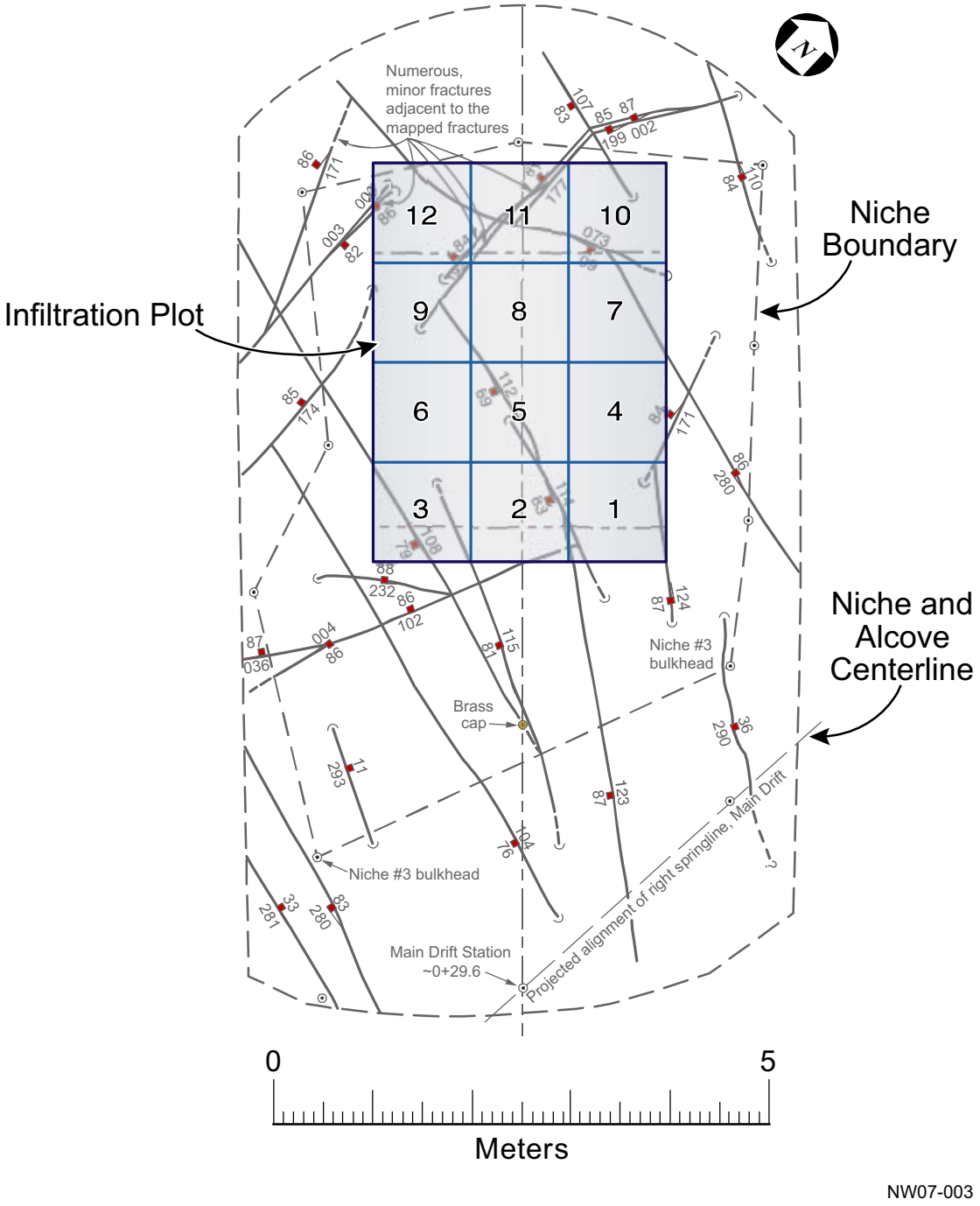

Source: DTN: GS030108314224.001 [DIRS 162131] with modification; Zhou et al. 2006 [DIRS 178226], Figure 1.

NOTE: The numbers and squares stand for strike and dip of fractures and location measured.

Figure 6.1-2. Schematic Illustration of the Infiltration Zones along the Floor of Alcove 8 Large-Plot Test with the Numbers Identifying the 12 Infiltration Subplots

The ponded infiltration test along the 12 subplots began in August 2002 and continued until October 2004 (DTNs: GS040308312242.001 [DIRS 176441]; GS050608312242.003 [DIRS 176442]; GS050408312242.002 [DIRS 176443]; GS050608312242.004 [DIRS 176444]). During this period, there were three distinct stages of liquid release. Stage 1 began with the ponding of the 12 subplots and continued through March 2003. During Stage 2, which extended from March 2003 until August 2003, water was ponded in subplots 2 and 12 while the surface of the remaining 10 subplots was kept free of standing water. Stage 3 began in August 2003, when ponded water was reintroduced in the 10 subplots. During this phase, in six of the subplots, the infiltration was briefly terminated and the surface was scrubbed to remove biofilms that had developed.

To facilitate the application of tracers, the infiltration plot was divided into three zones. In each zone, two separate tracers were introduced under ponded conditions on March 1, 2004. Table 6.1-1 summarizes the subplots in each zone, as well as the type of tracer and duration of tracers applied to the subplots. Radionuclide transport in the UZ is expected to experience physical processes some of which are similar to those for transport of these tracers (such as advection and matrix processes).

Table 6.1-1. Plots Combined to Form Specific Zones and Duration of Tracer Application in Each Zone

Zone	Stations/Plots in Zone	Start Date	End Date	Tracers
1	Plot 1, Plot 2	3/1/2004	4/13/2004	2, 6-Difluorobenzoic Acid Potassium Iodide
2	Plot 3, Plot 4, Plot 5, Plot 6, Plot 7, Plot 8, Plot 9	3/1/2004	3/17/2004	2, 5-Difluorobenzoic Acid Calcium Bromide
3	Plot 10, Plot 11, Plot 12	3/1/2004	4/13/2004	2, 4, 5-Trifluorobenzoic Acid Potassium Fluoride

Source: DTN: MO0511UCC011JB.002 [DIRS 176334].

Within the fractured rock, changes in saturation (and water potential) were monitored using boreholes drilled around Niche 3 to monitor water-front travel times. Within each borehole, electrical resistivity probes recorded the electrical resistivity of fracture water over the entire test period. The observed travel times from these boreholes are given in the file *Travel time for predictive model1.xls* in DTN: LB0308A8N3TRTM.001 [DIRS 176448].

Seepage was collected at the ceiling of Niche 3 by a capture system (Figure 6.1-5) consisting of compartments constructed of transparent lexan plastic. Water dripping into each of the tray units was collected into a container connected with the tray unit; the container was in turn connected to a pressure transducer used to remotely monitor seepage rates and volume, and the seepage rates (in L/day) were recorded for the container. The seepage rates in different tray units reflected the spatial variability in the seepage on the niche ceiling. To minimize the effects of evaporation resulting from the Main Drift ventilation, the bulkhead door at the entrance to the niche was closed and sealed.

6.1.2 Testing Observations

As previously indicated in Section 6.1.1, infiltration (water release) consists of three stages. Stage 1 of the infiltration experiment extended over a period of 216 days. The infiltration response measured at various locations along the plot indicates that there was large spatial and temporal variability in the movement of water through the 3×4 m^2 surface (Figures 6.1-3 and 6.1-4).

Stage 2 of the test was designed to evaluate the impact of neighboring subplots on infiltration rates. To achieve this, at the start of Stage 2, water was removed from 10 of the 12 subplots, while in the two subplots with the highest near-constant infiltration rates (i.e., subplots 2 and 12), ponding continued uninterrupted. For the duration of this stage, which extended for a period of 157 days, this upper boundary condition was maintained along infiltration plots 2 and 12, respectively. Measured fluxes in these subplots suggest that infiltration in the subplots was not significantly impacted when the adjacent subplots were dried.

Stage 3 of the infiltration test was configured to evaluate the impact of two specific perturbations on infiltration rates. For the first, the supply of water to individual plots was terminated for varying periods. The second perturbation involved the removal of a thin layer of biomass that had grown over the infiltration surface from six of the 12 subplots. Specifically, selected subplots were scrubbed on two occasions. On August 23, 2004 (734 days), scrubbing was performed on the surfaces of Subplots 2 and 3. And a few weeks later on September 13 to 14, 2006 (755 to 756 days), subplots 1, 6, 9, and 12 were also scrubbed (Figure 6.1-4).

When ponded infiltration was resumed along the entire plot during Stage 3, the surface of 10 of the 12 subplots had been dry for approximately five months, while the remaining two (i.e., subplots 2 and 12) had been dry for approximately three weeks. With the resumption of ponding, infiltration rates in 9 subplots (i.e., subplots 3 to 11), were found to be similar to those at the end of Stage 1. It appears that during the long dry period, the near-surface hydrologic properties in these 9 plots remained relatively unchanged, such that there was no measurable difference in the infiltration rates.

Subplots 1, 2 and 12 were the only plots that showed some impact of the dryout that preceded Stage 3. In subplot 1 the infiltration rate at the resumption of ponding was ~30 L/day, much higher than at the end of Stage 1 when it was ~5 L/day. However, the higher infiltration rates did not persist, and the daily flux along this subplot rapidly approached a relatively steady rate of ~10 L/day. In subplot 2, when water was reintroduced into the plot after three weeks of drying, the infiltration rates were initially slightly lower than at the end of Stage 2 (i.e., 12 L/day, versus 14 L/day), but steadily increased to 30 L/day in the next 30 days. The infiltration rate then began to decline gradually, reaching a near-constant rate of 12 L/day approximately 200 days after Stage 3 ponding began. In Subplot 12, the infiltration was about 15 L/day at the end of Stage 2, and then it took over 150 days for the plot to achieve the same infiltration rate.

When ponded water was briefly removed from subplots 1, 6, 9, and 12, 734 days after the start of the infiltration experiment, there was no measurable difference in infiltration rates once ponding was resumed a few hours later. Similarly, in subplots 3, 6, 9, and 12, infiltration rates did not change after the surface of each of these plots had been briefly scrubbed.

Subplots 1 and 2 were the only plots that showed a measurable response to scrubbing of their surfaces. Subplot 1, which had not shown any response to a brief interruption in the supply of ponded water, responded almost immediately after the surface had been cleaned. Here, the near-constant infiltration rate of ~5 L/day that had persisted for over a year rapidly increased over the next five days before peaking at ~110 L/day. After peaking, the infiltration rates then rapidly decreased over the next 30 days, during which ponded conditions were maintained along the plot. Although Alcove 8 subplots 1 and 2 are located relatively close to the mapped fault [BSC 2004 [DIRS 170004], Figure 6.12.4-1], the presence of the fault appears to have little influence on the test results, because for entire duration of the test, no corresponding seepage was observed along the fault trace in Niche 3.

In subplot 2, the infiltration rate increased from ~12 L/day to 20 L/day, immediately after the plot was scrubbed on day 734 of the test (Figure 6.1-3). Following this steep increase, infiltration rates gradually increased to 30 L/day in the next 12 days, and then sharply to 70 L/day over a period of nine days before dropping to ~30 L/day over a period of 24 hours. This dramatically reduced infiltration rate coincided with perturbations to the surface of subplot 1 (Figure 6.1-3). As the infiltration rates jumped in subplot 1, they dropped in subplot 2, suggesting that there was some mechanism by which flow through the surface of subplot 2 was reduced as the permeability of the surface of subplot 1 was increased. The reduced infiltration rates in subplot 2 persisted for the next 30 days before gradually declining over the remaining few days of the test. The total infiltration rate as a function of time is presented in Figure 6.1-4.

Seepage was first visually observed in Niche 3 on September 10, 2002, on the back wall where the wall meets the ceiling. Measurable seepage was recorded for a week after these initial observations. Early seepage was measured approximately 30 days after the initial application of water along the infiltration plot (Figure 6.1-6). The ceiling of Niche 3 is divided into 12 zones with the about same coverage areas (called columns in Figure 6.1-5). One zone may cover one or more seepage tray units (Figure 6.1-5). This is because a regular numerical mesh and regularly distributed property domains (columns) are used in the model, while the seepage trays have varied cover areas. The seepage rates are presented here for each zone (column) in Figure 6.1-6, because these are the data directly used in model calibrations (Sections 6.2 and 6.3). Following the arrival of the wetting front, seepage at most monitored locations appeared to increase over a period of about one to four weeks before gradually decreasing. The highest total seepage rates measured during this peak event were about 30 L/day (Figure 6.1-7). Following peak values, the seepage rates at all locations continuously decreased, with maximum rates measured at about 5 L/day in March of 2003 (Figure 6.1-7).

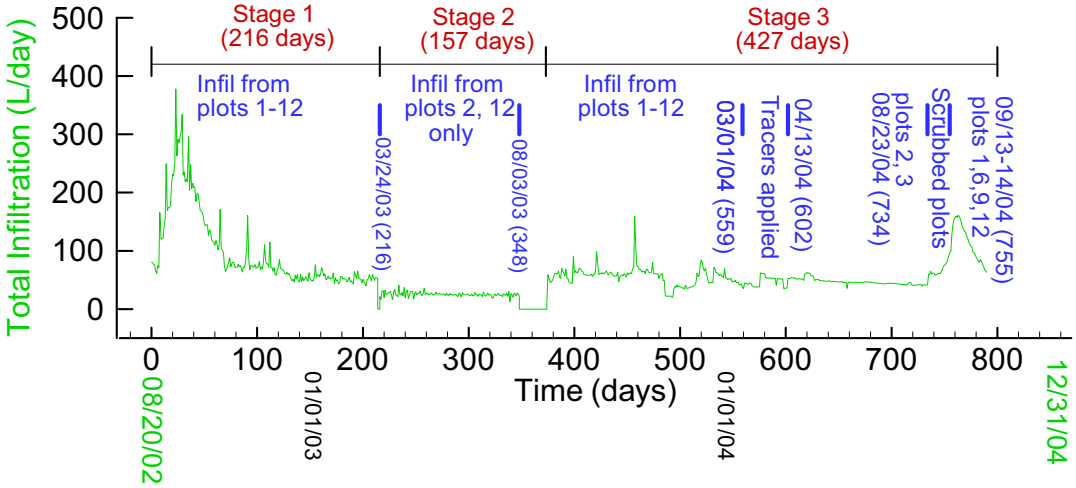

Source: DTNs: GS040308312242.001 [DIRS 176441]; GS050608312242.003 [DIRS 176442]; GS050408312242.002 [DIRS 176443]; GS050608312242.004 [DIRS 176444].

NOTE: Data processing procedures are given in Appendix B.

Figure 6.1-4. Total Infiltration Rate as a Function of Time

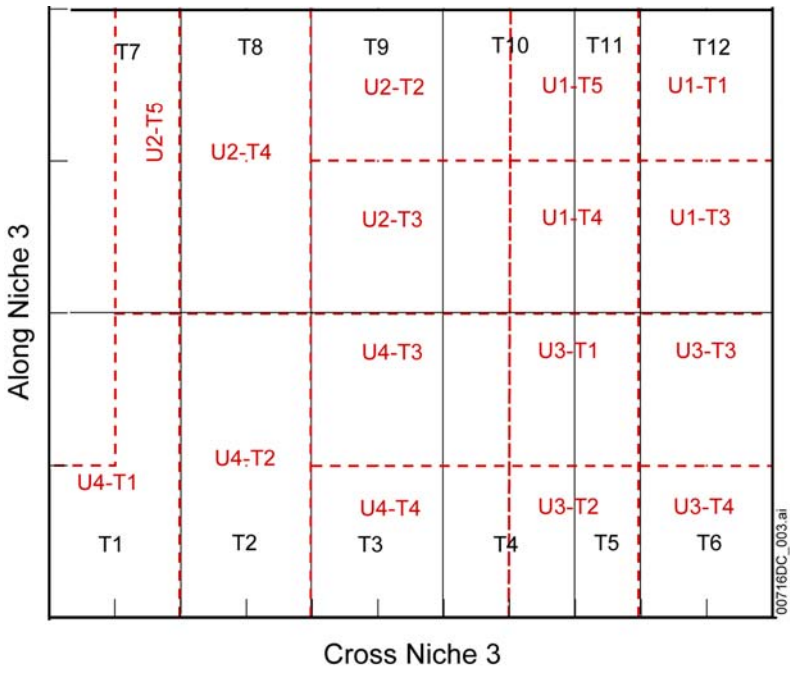

Source: Output DTN: LB0602A8N3FTR0.001; Lu 2006 [DIRS 176702], p. 20.

NOTE: Black solid lines delineate the column boundaries, and red dashed lines the seepage tray unit's boundaries.

Figure 6.1-5. Schematic Configuration of the Seepage-Collection System and Boundaries of the Columns (T1 to T12)

When water was released into only two of the 12 subplots, the seepage rate dropped to very small values over a period of two months. When infiltration was resumed on all 12 plots in late August 2003, after a lag of about 30 days the seepage rates quickly climbed to 10 to 15 L/day. Over the next five months, daily seepage rates fluctuated significantly more than observed earlier, and then after January 2003, these rates gradually dropped to near zero. The total seepage rate as a function of time is presented in Figure 6.1-7.

Tracer concentrations in seeping water collected at Niche 3 were measured after tracers were injected from infiltration plots at Alcove 8. The measured results are presented in Figure 6.1-8. Note that essentially no tracer concentrations (excluding background concentrations) were observed until the infiltration pulse occurred, owing to scrubbing of the infiltration plots. Also note that the observed relative concentrations (the concentration divided by the average concentration of injected tracer at the infiltration plots) are small for these breakthrough signals. Further discussion of these tracer data is given in Section 6.2.4.

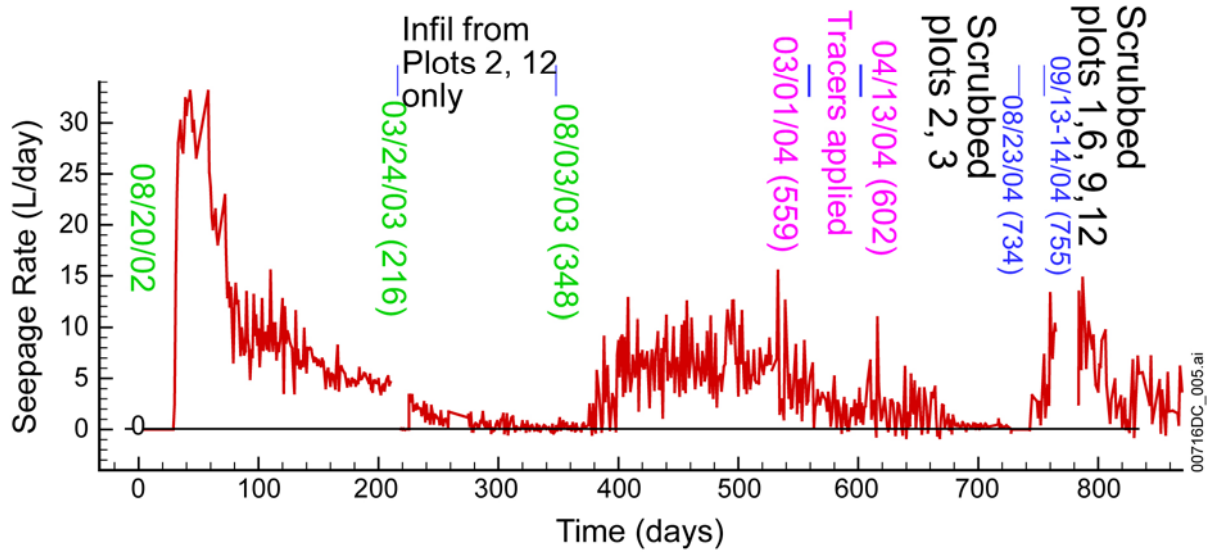

Source: DTNs: LB0507A8N3SEEP.001 [DIRS 176445]; LB0507A8N3SEEP.002 [DIRS 176446]; LB0507A8N3SEEP.003 [DIRS 176447]; LB0308A8N3SEEP.001 [DIRS 166090]; LB0312A8N3MDLG.001 [DIRS 169761].

NOTE: Data processing procedures are given in Appendix B.

Figure 6.1-7. Total Seepage Rate as a Function of Time

6.2 PRE-TEST PREDICTION OF LATE STAGE OF THE TESTS

As described in Section 6.1, the Alcove 8/Niche 3 tests consisted of several different stages. Based on test data from the earliest stage of the tests (for the first 210 days), a numerical model for flow and transport at the test site was developed. During that stage of the tests, water was applied in all of the 12 infiltration plots. The seepage and infiltration-rate data (collected from that stage of the tests) were used to calibrate the model to obtain the site-specific rock properties. The calibrated model was then used to predict results for subsequent tests planned at that time. A comparison of predicted and observed test results provides a useful way to evaluate the methodology used for modeling UZ flow and transport processes and to improve understanding of physical mechanisms behind those processes in the UZ. This subsection documents the development of the model for pre-test prediction and a comparison between observed and predicted test results.

Note that the pre-test prediction discussed here is the updated pre-test prediction. An initial version of pre-test prediction was documented in *Pre-Test Predictions of Alcove 8 –Niche 3 Cross-Over Test* (BSC 2001 [DIRS 155827]). Because the test conditions were later considerably adjusted during actual tests and some site-specific data were available at the early stage of the tests, a numerical model, as previously discussed, was developed to more accurately account for the test conditions and calibrate against the test data available at that time (BSC 2004 [DIRS 169861], Section F2.1). The model was then used to provide pre-test predictions for the subsequent tests (including tracer tests). The updated pre-test prediction results are contained in DTN: LB0312A8N3MDLG.001 [DIRS 169761].

6.2.1 Model Development

A three-dimensional numerical grid was constructed for modeling the large-plot tests (Figure 6.2-1) (DTN: LB0312A8N3MDLG.001 [DIRS 169761]). The top of the grid corresponds to the floor of Alcove 8, where infiltration occurred. The 12 infiltration plots and the projected outline boundary of the Niche 3 ceiling (under which seepage trays were installed) are also shown in Figure 6.2-1. Small grid sizes were used above the niche ceiling and near the interface between model layers tsw33 and tsw34, to capture diverted water flow around the niche and rock-property transition at the interface between model layers. (Model layers tsw33 and tsw34 correspond to upper lithophysal and middle nonlithophysal geological units.) For simplicity, the niche ceiling was approximated as a flat surface. To capture the transient flow and transport behavior, the multiple interacting continua (MINC) model (Pruess and Narasimhan 1985 [DIRS 101707]) was used. The MINC model can handle steep pressure and concentration gradients near fracture–matrix interfaces. In the numerical grid shown in Figure 6.2-1, each gridblock includes one fracture element and five matrix elements. The grid spacings for the five matrix elements are 0.004 m, 0.027 m, 0.073 m, 0.143 m, and 0.472 m for tsw33, and 0.003 m, 0.019 m, 0.051 m, 0.099 m, and 0.326 m for tsw34, respectively (DTN: LB0312A8N3MDLG.001 [DIRS 169761], file: *SrunA*). The smallest grid spacing corresponds to the elements closest to fractures.

To handle the spatial variabilities observed from both the infiltration rates at Alcove 8 and seepage rates at Niche 3, heterogeneous distributions of fracture properties within a given model layer were considered in the three-dimensional model. Within a model layer, fractured rock is

divided into a number of vertical columns within zones below the infiltration plots (for tsw33) or above the ceiling of Niche 3 (for tsw34). Therefore, there are two sets of vertical columns that are located in tsw33 and tsw34, respectively. Each column corresponds to an infiltration plot (in tsw33) or one or more adjacent seepage collection units (in tsw34). The rest of the rock was considered to have homogeneous property distributions within each model layer. The homogeneous property distributions were also used for each column (Section 6.2.2). Also note that for tsw33, the column numbers (Table 6.2-1) are the same as infiltration plot numbers (Figure 6.1-2). For example, Column 1 corresponds to the first infiltration plot for tsw33.

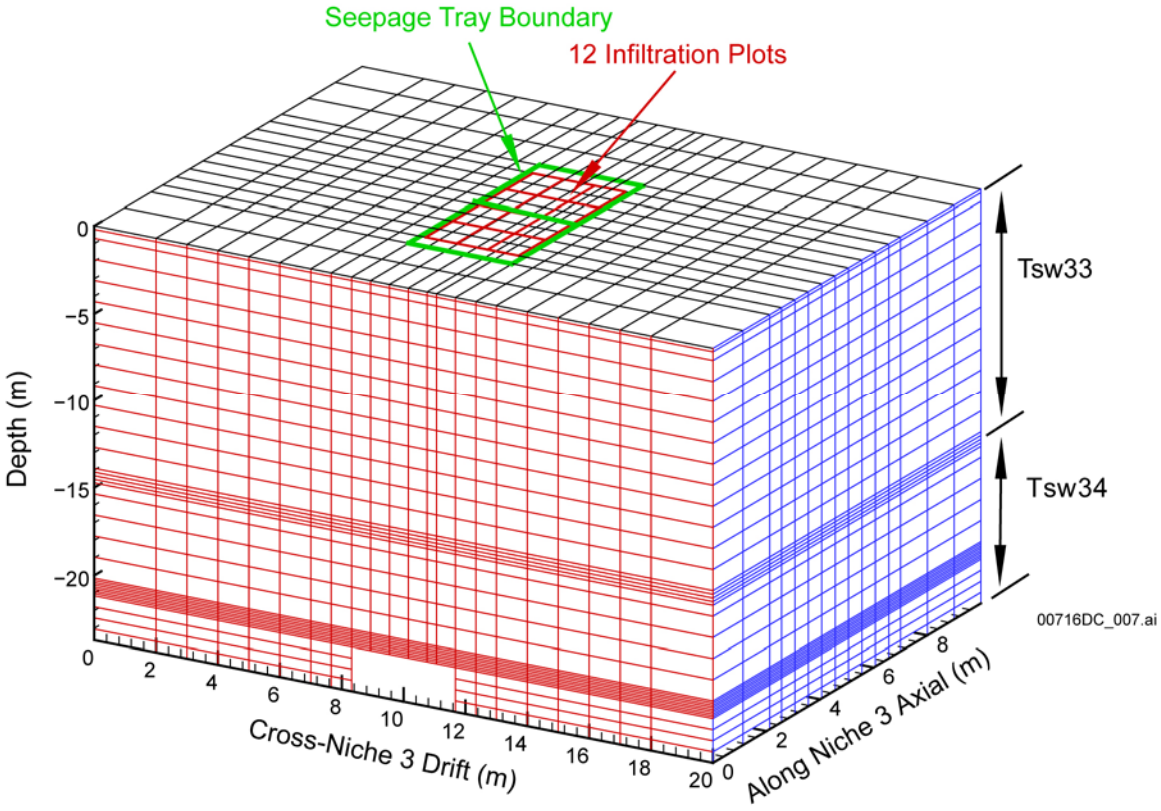

3-D MINC Mesh: 67,320 Elements (22×15×34×6), 140,000 Connections

Source: DTN: LB0312A8N3MDLG.001 [DIRS 169761]; BSC 2004 [DIRS 169861], Figure F-1.

Figure 6.2-1. Illustration of Three-Dimensional Numerical Grids for the Large-Plot Tests

Previous fracture-network modeling demonstrated that unsaturated flow paths within a fracture network are generally vertical (as a result of gravity-dominated flow behavior) (Liu et al. 2002 [DIRS 160230]), supporting the use of the column-based heterogeneous distributions. Use of these vertical columns are appropriate to approximately capture flow behavior associated with these flow paths. Another consideration for using the simple column-based approach is data limitation. As in any field test in the area of subsurface hydrology, not enough data are available for characterizing detailed flow paths between Alcove 8 and Niche 3. A simple model of

Then the original test condition (ponded release of water to 12 infiltration plots) were restored. After approximately steady-state infiltration and seepage processes were re-established, different tracers were simultaneously introduced into the infiltrating water applied at different infiltration plots (Table 6.1-1). Table 6.2-2 gives the information regarding tracers used. In all the tracer tests, tracer concentrations as a function of time were analyzed for water samples collected at Niche 3. The definitions of infiltration zones are given in Table 6.1-1.

Seepage rate data collected for the first 210 days (after the large-plot tests started) were used for model calibration (Section 6.2.2). The calibrated model was used to predict test results after the first 210 days. Then, forward simulations using iTOUGH2 V5.0 were performed for predicting seepage rates, and T2R3D V1.4 was used for simulating tracer transport. The dispersion process was ignored in tracer simulations, because the dispersion process is not considered to be important for the test conditions (Liu et al. 2003 [DIRS 162470]). Again, following Moridis et al. (2003 [DIRS 161902], Table 1), the tortuosity factor for the tuff matrix is approximated by the corresponding matrix porosity.

Figure 6.2-4 shows simulated and observed total seepage rates. Figure 6.2-5 presents the corresponding simulated and observed seepage rates for different vertical rock columns corresponding to individual seepage trays. The model calibration matches observed seepage rates for most rock columns except column 7 (the model calibration gives essentially zero seepage rate for column 7). Shown in Figures 6.2-6 through 6.2-8 are predicted tracer breakthrough curves for different vertical rock columns. These predicted tracer breakthrough curves are also compared with relative tracer concentration measurements determined as the ratio of differences between measured concentration values (Figure 6.1-8) and the background concentration for the given tracer to the difference between the applied tracer concentration values in the infiltration plots (Figure 6.1-8) and the background concentration. Since no breakthrough signal was observed for the first 100 days after the tracer test started, the background concentration for a given tracer was determined as the average measured concentration of seeped water for these 100 days. Note that in pre-test predictions (Figures 6.2-4 to 6.2-8), two phases of tests were assumed. Phase I corresponds to ponding conditions and Phase II to hypothetical future nonponding water-release conditions. Since Phase II was not actually implemented in tests, it will not be discussed in the remainder of this report.

Table 6.2-2. Information for Tracers Used in Phase I Tests

Tracer Number	Tracer Name	Molecular Diffusion Coefficient (m^2/s)	Infiltration Zone Number	Duration of Tests (days)
1	2,6-Difluorobenzoic Acid (DFBA)	8.1×10^{-10}	1	55.08
2	Potassium Iodide	2.045×10^{-9}	1	55.08
3	2,5-Difluorobenzoic Acid (DFBA)	8.1×10^{-10}	2	36.46
4	Calcium Bromide	2.080×10^{-9}	2	36.46
5	2,4,5-Trifluorobenzoic Acid (TFBA)	7.9×10^{-10}	3	55.49
6	Potassium Fluoride	1.475×10^{-9}	3	55.49

Source: DTN: LB0312A8N3MDLG.001 [DIRS 169761].

NOTE: The matrix diffusion coefficient values refer to those for anions for tracers 2, 4, and 6.

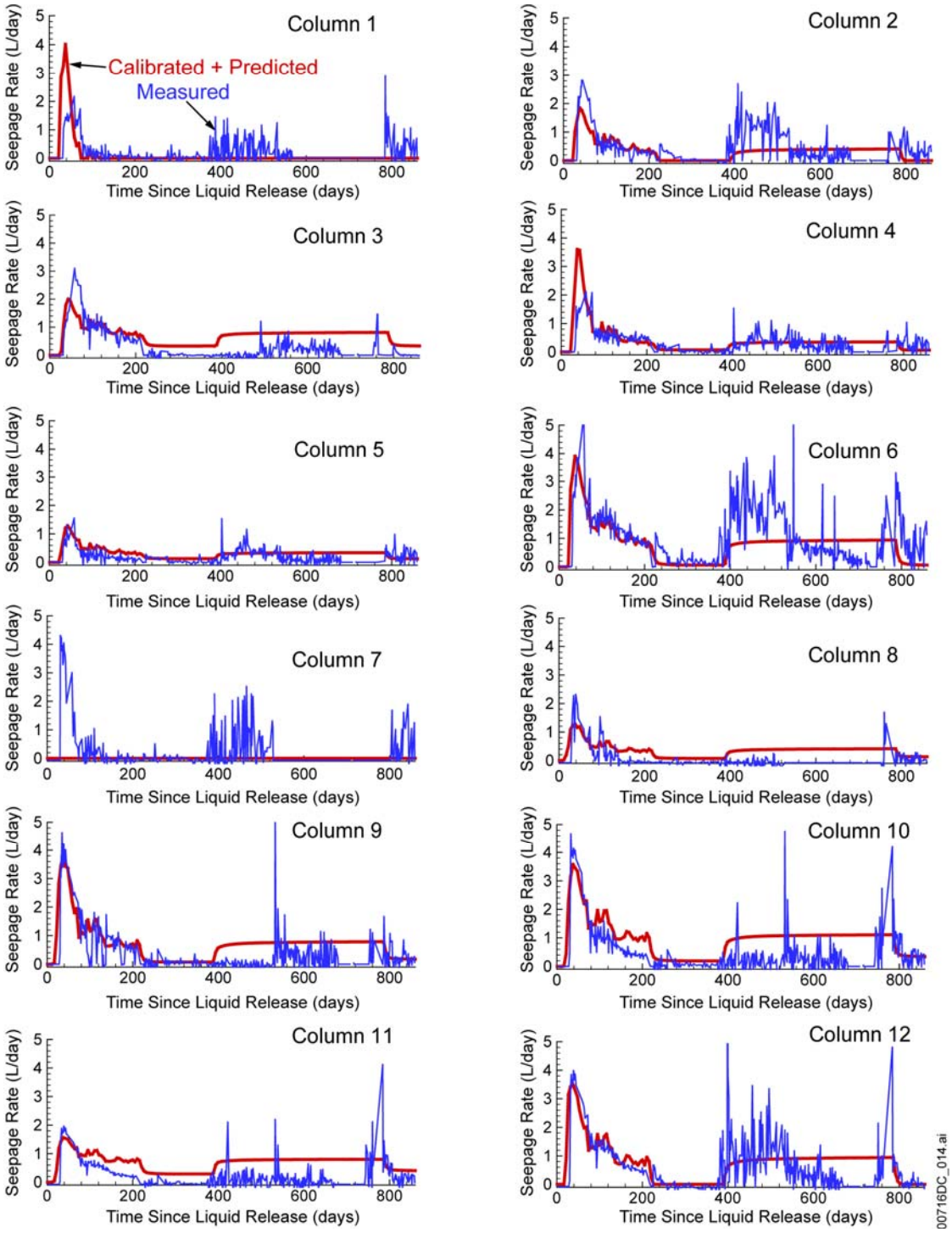

Source: DTNs: LB0312A8N3MDLG.001 [DIRS 169761]; LB0507A8N3SEEP.001 [DIRS 176445]; LB0507A8N3SEEP.002 [DIRS 176446]; LB0507A8N3SEEP.003 [DIRS 176447]; LB0308A8N3SEEP.001 [DIRS 166090].

NOTE: The observed seepage rate data used for model calibration are also shown here.

Figure 6.2-5. Simulated (red) and Observed (blue) Seepage Rates for Different Vertical Rock Columns

period between 740 days and the end of the tests, when effects of the infiltration pulses on seepage were observed. At this stage, reliable tracer breakthrough signals were observed for tracers introduced from Zone 1 (I^- and 2,6 DFBA) (Table 6.1-1). The seemingly much later breakthrough of I^- signal than 2,6DFBA may result from the very coarse interval between the last two samplings. Breakthrough signals for the other tracers are not considered reliable, based on the following two considerations: First, there might be a significant measurement error for low concentrations (on the order of 0.1 ppm) of organic tracers 2,4,5 DFBA and/or 2,5 DFBA. For example, the measured concentrations of 2,4,5 DFBA before the tracer injection are on the same order of magnitude of the observed concentration at later times (Figure 6.1-8), while the tracer concentration before the injection is supposed to be zero. Second, no obvious breakthrough signals were observed for the inorganic tracers (F^- and Br^-) that were simultaneously injected into the same infiltration plots with the two organic tracers mentioned above. The tracers introduced from Zone 1 (I^- and 2,6 DFBA) do not have those problems. On the other hand, the tracer breakthrough signals were observed right after the infiltration pulse from Zone 1 as a result of scrubbing infiltration plots. The mechanisms for tracer transport related to the observed breakthrough signals are not entirely clear at this time. There are two possible interpretations for these signals. The biofilms near the infiltration plots (Zone 1) might (chemically and/or physically) adsorb a certain amount of tracers (especially organic tracers). During the scrubbing, the films were disturbed, resulting in the release of the tracers. The tracers were then transported to Niche 3 along relatively fast flow paths, owing to the significant increase in infiltration rate in Zone 1 after the scrubbing. Another possible interpretation is related to the changes in flow paths during the tests as a result of particle movement. During the tracer application period, some flow paths (with tracers) stopped conducting water, leaving the traced water in some dead zones while new flow paths started to conduct water. The infiltration pulse resulting from the scrubbing might have made the "dead" flow paths active again and washed the "entrapped" traced water into Niche 3. Nevertheless, it is difficult to meaningfully model these observed tracer breakthrough signals for I^- and 2,6 DFBA, because the amount of tracers (contributing to the signals) and tracer locations before the scrubbing are unknown.

Based on the above discussion, a comparison is made between the pre-test prediction and observed results for tracer transport (between the time when the tracers were injected and about 740 days into the test when an infiltration pulse occurred as a result of scrubbing infiltration plots). Essentially no concentrations of the applied tracers excluding the background concentrations were observed during the time period, while considerable concentrations for different tracers as a function of time are predicted. An important reason for this discrepancy is that matrix diffusion may be underestimated in the pre-test prediction. Model analyses of test results based on the conceptual understanding of the test data (discussed in this subsection) and the related uncertainties will be further discussed in sections to follow.

6.3 MODELING ANALYSES OF TEST RESULTS

As previously discussed in Section 6.2.2, the seepage data collected at an early stage of the tests were used to calibrate the initial version of the numerical model used for the pre-test predictions of the subsequent tests. To better understand the flow and transport processes at the test sites and obtain more representative site-specific rock properties, it is necessary to calibrate the model with additional data that became available subsequently. This subsection documents the model calibration with all the infiltration and seepage data. Two different conceptual models for water

flow at the test site were considered. The sensitivity study on tracer transport was performed using the calibrated models.

6.3.1 Model Calibration with All the Available Infiltration and Seepage Data

The model developed in Section 6.2 was refined by further model calibrations using all the infiltration and seepage data. Observed flow and transport data at the test site exhibit very complex features (such as a large degree of temporal variability in seepage rate) that provide a significant challenge for model calibration.

To deal with uncertainties resulting from such complexities, different conceptual models were explored in the model calibration process. The base-case conceptual model is the same as that used for the pre-test prediction and considered flow paths from all the infiltration plots to be connected to the ceiling of Niche 3. However, during the testing period, when infiltrating water was applied to plots 2 and 12 only, the observed seepage rates are close to zero (Figure 6.1-6). Therefore, it is possible that only a small amount of water from these two infiltration plots contributed to seepage rates observed from Niche 3. The alternative conceptual model is that flow paths from infiltration plots 2 and 12 did not contribute to the seepage into Niche 3. To implement this conceptual model, zero infiltration rates were used for the two plots when simulating the seepage into the niche.

Model calibration procedures were the same as those described in Section 6.2.2, except that all the infiltration rate and seepage rate data collected over the whole test period were used for each conceptual model. Matches between simulated and observed seepage rates and calibrated properties are presented in Figures 6.3-1 (output DTN: LB0602A8N3FTR0.001, file: *SrunAflowci.tec*) and 6.3-2 (output DTN: LB0602A8N3FTR0.001, file: *try1i.tec*), and Tables 6.3-1 (output DTN: LB0602A8N3FTR0.001, file: *SrunAflowci.par*) and 6.3-2 (output DTN: LB0602A8N3FTR0.001, file: *try1i.par*), respectively. Given the complexity of the problem, matches are considered fairly reasonable. Different conceptual models give generally similar matches (especially for the total seepage rates), although the base-case conceptual model gives a better match. This highlights the need to develop multiple conceptual models for test-result interpretation, because the use of different conceptual models with similar matches can cover a relatively large range of flow behavior, and therefore may be able to better capture (or bound) the actual flow processes.

Table 6.3-2. Calibrated Rock Properties for the Alternative Conceptual Model

Model Layer		Permeability (m^2)	van Genuchten α (Pa^{-1})	van Genuchten m	Porosity
tsw33	Column 1	0.1396×10^{-12}	0.5873×10^{-3}	0.608 [(a)]	0.066 [(a)]
	Column 2	0.2370×10^{-12}			
	Column 3	0.4163×10^{-13}			
	Column 4	0.4425×10^{-13}			
	Column 5	0.8968×10^{-13}			
	Column 6	0.2596×10^{-13}			
	Column 7	0.1849×10^{-13}			
	Column 8	0.9505×10^{-13}			
	Column 9	0.3474×10^{-13}			
	Column 10	0.1377×10^{-12}			
	Column 11	0.2622×10^{-12}			
	Column 12	0.4687×10^{-13}			
	Rest rock mass	0.1224×10^{-11}	0.2287×10^{-2}		
tsw34	Column 1 (upper)	0.1497×10^{-12}	0.1821×10^{-2}	0.608 [(a)]	0.010 [(a)]
	Column 2	0.2796×10^{-12}	0.2719×10^{-2}		
	Column 3	0.4060×10^{-12}	0.4776×10^{-2}		
	Column 4	0.2304×10^{-12}	0.4114×10^{-2}		
	Column 5	0.8821×10^{-13}	0.2982×10^{-2}		
	Column 6 (upper)	0.4008×10^{-12}	0.1653×10^{-2}		
	Column 7	0.2448×10^{-12}	0.2042×10^{-2}		
	Column 8	0.7955×10^{-12}	0.2295×10^{-2}		
	Column 9	0.2874×10^{-11}	0.2428×10^{-2}		
	Column 10	0.6997×10^{-12}	0.1472×10^{-2}		
	Column 11 (upper)	0.2642×10^{-11}	0.1425×10^{-2}		
	Column 12 (upper)	0.4687×10^{-13}	0.5873×10^{-3}		
	Rest rock mass	0.4704×10^{-12}	0.4233×10^{-3}		
	Column 1 (lower)	0.5012×10^{-12} [(a)]	0.1000×10^{-2}		
	Column 6 (lower)	0.5012×10^{-12} [(a)]	0.6059×10^{-2}		
	Column 11 (lower)	0.5012×10^{-12} [(a)]	0.5175×10^{-2}		
	Column 12 (lower)	0.5012×10^{-12} [(a)]	0.3911×10^{-2}		

Source: Output DTN: LB0602A8N3FTR0.001.

[(a)] These properties are not varied during model calibration.

6.3.2 Sensitivity Study of Tracer Transport

The calibrated flow fields (output DTN: LB0602A8N3FTR0.001) were used as input to tracer transport simulations performed with T2R3D V1.4. The simulation procedure is the same as that used for pre-test prediction. The molecular diffusion coefficients for the tracers shown in Table 6.2-2 were employed in the simulations. Based on analyses of the relevant diffusion experiment results, Moridis et al. (2003 [DIRS 161902], Table 1) reported that the tortuosity factor for the tuff matrix could be approximated by the corresponding matrix porosity. Like the pre-test

For the alternative conceptual model, only the organic tracers were used in simulations because they have smaller matrix diffusion coefficients than those for inorganic tracers. For a given zone (Table 6.2-2), a smaller diffusion coefficient is expected to give a higher peak concentration value, as demonstrated in Figures 6.3-3 and 6.3-4. Since the purpose here is to show the conditions under which tracer concentrations are so low that they might not be detected in practice, it is adequate to simulate tracers with lower diffusions only (for a given zone). It also should be noted that the discussed relation between the peak concentration and diffusion coefficient (Table 6.3-3) is not always observed for the base-case conceptual model. This is because the simulated tracer concentrations are so low that round-off errors in the simulations may considerably impact the simulation results, which, however, does not change the finding that the increased matrix diffusion coefficient is needed to explain the field observation.

Table 6.3-3. Simulated Peak (Relative) Concentrations Monitored at Niche 3 for the Increased Matrix Diffusion Coefficients

Tracer	Base-Case Conceptual Model	Alternative Conceptual Model
I^-	1.60×10^{-4}	—
Br^-	7.30×10^{-6}	—
F^-	7.14×10^{-5}	—
2,6 DFBA	1.71×10^{-3}	1.17×10^{-4}
2,5 DFBA	6.05×10^{-5}	2.37×10^{-3}
2,4,5 DFBA	3.98×10^{-6}	1.04×10^{-3}

Source: Output DTN: LB0602A8N3FTR0.001.

6.4 DISCUSSIONS

Modeling analysis of the Alcove 8/Niche 3 test provides an important opportunity to improve the current understanding of UZ flow and transport at the Yucca Mountain site, although a considerable degree of uncertainty remains. While a number of issues related to the tests and modeling analyses have been touched on in previous subsections, this subsection documents further discussions of the test and modeling results and their implications.

6.4.1 Effective Matrix Diffusion Coefficient and Its Enhancement

The comparison of observed and simulated test results (Section 6.3) suggests that the use of matrix diffusion coefficient measured at a small-scale underestimates the retardation of tracer transport at the test site. The effective matrix diffusion coefficient (molecular diffusion coefficient in free water multiplied by matrix tortuosity) is a key parameter for describing matrix diffusion that generally results in retardation. Matrix diffusion refers to solute transport from fracture networks into the surrounding matrix blocks resulting from molecular diffusion (Neretnieks 1993 [DIRS 123099], pp. 47 to 48). Mass transfer between fractures and the tuff matrix plays an important role in transport within the UZ. Because the flow velocity in the matrix is much slower than in fractures, transfer of tracer from fractures to the matrix can significantly retard overall tracer transport.

This result is consistent with findings from a number of studies published in the literature (Shapiro 2001 [DIRS 162132]; Neretnieks 2002 [DIRS 162140]; Liu et al. 2003 [DIRS 162470]; BSC 2004 [DIRS 169861], Section 7.6). Effective matrix-diffusion-coefficient values have been estimated from a number of field test sites characterized by different rock types. Neretnieks (2002 [DIRS 162140]) reported matches to tracer test data collected from the Äspö site with a test scale of 5 m and found a need for a factor 30 times larger for the fracture–matrix interface area (or effective matrix-diffusion coefficient) than expected. Note that the increase in fracture–matrix interface area is equivalent to the increase in effective diffusion coefficient (for a given interface area in a model). Interestingly, Neretnieks (2002 [DIRS 162140]) also indicated that nine other research groups had also independently evaluated the tracer test data from the site using different modeling approaches. Nearly all the groups found the need for a factor 30 to 50 times larger effective fracture-matrix interface area (or effective matrix-diffusion coefficient) than expected.

Liu et al. (2003 [DIRS 162470]) and *UZ Flow Models and Submodels* (BSC 2004 [DIRS 169861], Section 7.6) presented model analyses of two different sets of field test data, collected in the unsaturated zone of Yucca Mountain. Unlike studies reported by other researchers mentioned in this subsection, Liu et al. (2003 [DIRS 162470]) and *UZ Flow Models and Submodels* (BSC 2004 [DIRS 169861], Section 7.6) matched both the flow field (characterized by water travel time and/or seepage into subsurface openings) and tracer breakthrough curves. They reported that increased fracture–matrix interface areas (or effective matrix diffusion coefficients) were needed for both tests.

Becker and Shapiro (2000 [DIRS 169947]) and Shapiro (2001 [DIRS 162132]) reported analyses of tracer test data from fractured crystalline rock at the Mirror Lake site. Becker and Shapiro (2000 [DIRS 169947]) showed that laboratory measurement of the effective diffusion coefficient should be replaced by the coefficient in free water to match the bromide data in their Test C with a test scale of about 36 m. However, they were not able to match all the breakthrough curves for different tracers, and argued that advective transport processes contribute to this discrepancy. An alternative explanation may be that the simple model used by those authors cannot capture all the importance processes (such as effects of subsurface heterogeneity), even when matrix diffusion is a dominant process. Shapiro (2001 [DIRS 162132]) found that matrix diffusion coefficient values three to five orders of magnitude greater than the estimates of the matrix diffusion coefficient from laboratory experiments were needed to match the tracer data observed at a kilometer scale. His analysis probably provides the first estimate for kilometer-scale effective diffusion coefficient.

In the studies mentioned above, the matrix diffusion coefficients were estimated by fitting the observed breakthrough curves, which generally involves a certain degree of parameter uncertainty due to the non-uniqueness of the curve-fitting procedure. Most recently, Lofgren and Neretnieks (2004 [DIRS 176479]) reported directly measured in situ formation factor values (for two boreholes in a fractured rock test site) as compared with lab measurements for rock samples. (The formation factor is proportional to the matrix diffusion coefficient.) The measurement was based on the Einstein analogy between molecular diffusion and ionic mobility, and the formation factor was estimated from measured electrical conductivity data. As indicated in their study (Lofgren and Neretnieks 2004 [DIRS 176479], Figures 3 and 4, Table 1), the in situ formation factor (or effective matrix diffusion coefficient) values are larger than those measured from rock

matrix sample or measurement intervals (within the boreholes) without connecting to a fracture network. Lofgren and Neretnieks (2004 [DIRS 176479]) also suggested that increased formation factors result from the existence of open, but hydraulically non-conducting fractures containing immobile water that acts as a preferential diffusion path.

Enhancement of the effective matrix diffusion coefficient reported in this study is also consistent with study results in the saturated zone near the Yucca Mountain site. Two crosshole tracer tests involving the simultaneous injection of different tracers with different molecular diffusion coefficients were conducted in two different intervals at the C-wells complex near the Yucca Mountain site (Reimus et al. 2003 [DIRS 162950]). The test scale (the distance between injection and monitoring boreholes) is on the order of 30 m. Transport parameters were estimated from the test results. In the original analysis by Reimus et al. (2003 [DIRS 162950]), a lumped parameter (combining effects of molecular diffusion coefficient, fracture aperture, and matrix porosity), rather than effective matrix diffusion coefficient, was estimated from fitting the test results. Values for the ratio of the effective matrix diffusion coefficient to the coefficient determined from rock matrix samples are determined using these estimated flow and transport parameters (Reimus et al. 2003 [DIRS 162950]), and by assuming intervals of flow channels observed from the corresponding boreholes to be the same as the spacing of conductive fractures (Appendix A). These ratios range from 5 to about 8, indicating the possible enhancement of effective matrix diffusion coefficient for the test site.

A number of researchers have attempted to explain why the effective matrix diffusion coefficient determined from field data is larger than the corresponding laboratory value (Shapiro 2001 [DIRS 162132]; Neretnieks 2002 [DIRS 162140]; Liu et al. 2003 [DIRS 162470]; BSC 2004 [DIRS 169861], Section 7.6). Shapiro (2001 [DIRS 162132]) suggested that kilometer-scale "effective matrix diffusion" is not a diffusive process, but actually an advective process between high and low permeability zones, resulting in a significantly large "effective diffusion coefficient." While this may be a plausible explanation, further confirmation is still needed. For example, Liu et al. (2003 [DIRS 162470]; see also BSC 2004 [DIRS 169861], Section 7.6) used a dual-permeability model involving both fast flow in fractures and slow flow in the matrix (as well as the advective transport between the two) and still found the need to use increased effective diffusion coefficients for matching the tracer test data. Neretnieks (2002 [DIRS 162140]) argued that existence of fracture in-filling creates relatively large areas for solute to diffuse into rock matrix, which, together with the process of diffusion into stagnant water, contributes to the need for increasing the effective diffusion coefficient to match the data. Wu et al. (2001 [DIRS 156399]) and Liu et al. (2003 [DIRS 162470]) indicated that the existence of many small-scale fractures (which considerably increase the fracture–matrix interface area, but are not considered in numerical models) may be the major reason for the relatively large effective diffusion coefficient calculated from field data. Lofgren and Neretnieks (2004 [DIRS 176479]) also suggested that the observed enhancement of effective matrix diffusion coefficient results from the existence of open, but hydraulically nonconducting fractures containing immobile water that acts as a preferential diffusion path.

It is very likely that the enhancement is due to a combination of different mechanisms (including those mentioned above). The major mechanism may be the complexity of flow path geometry in a fracture network that is largely ignored in the current modeling practices. Water flow in a single flow path (or channel) has often been simplified as a flow process within a single straight

tracers. There is not evidence in the literature to support that the tracers can be significantly entrapped by biofilms. Another possible explanation is based on the chaotic (unstable) flow behavior of unsaturated flow. After the tracers were applied, the flow paths to Niche 3 were dramatically shifted (due to unstable flow process) such that these flow paths were not connected to Niche 3. As a result, no tracer was observed in Niche 3 until the connection resumed by scrubbing the infiltration plots. This explanation sounds plausible, but is not supported by field observations. For example, the seepage data show that seepage rates had been stabilized for about 150 days after the tracer was introduced for columns 1 to 6 where the relatively large tracer concentrations were observed (Figures 6.3-1, 6.1-5, and 6.1-8).

Nevertheless, based on the current conceptual understanding of flow and transport at the test site, simulation results show that the actual, effective matrix diffusion coefficient should be much larger than the lab-scale value, which is consistent with study results published in the literature (Section 6.4.1). At the same time, it is useful to note that for the given uncertainties, the used enhancement factor of effective matrix diffusion coefficient (Section 6.3.2) may be considered as an upper limit in order to be conservative in modeling radionuclide transport in the UZ.

(2) The data on the geology, hydrology, and geochemistry of the unsaturated zone, are collected using acceptable techniques.

Approved QA procedures identified in the TWP (BSC 2006 [DIRS 177465], Section 4) have been used to conduct and document the activities described in this analysis report.

(3) Estimates of deep-percolation flux rates constitute an upper bound, or are based on a technically defensible unsaturated zone flow model that reasonably represents the physical system. The flow model is calibrated, using site-specific hydrologic, geologic, and geochemical data. Deep-percolation flux is estimated, using the appropriate spatial and temporal variability of model parameters, and boundary conditions that consider climate-induced change in soil depths and vegetation.

The numerical models used in this study were calibrated against infiltration and seepage rate data to determine the site-specific rock property data (Sections 6.2 and 6.3).

(6) Accepted and well-documented procedures are used to construct and calibrate numerical models.

Approved QA procedures identified in the TWP (BSC 2006 [DIRS 177465], Section 4) have been used to conduct and document the activities described in this analysis report.

(7) Reasonably complete process-level conceptual and mathematical models are used in the analyses. In particular: (i) mathematical models are provided that are consistent with conceptual models and site characteristics; and (ii) the robustness of results from different mathematical models is compared.

The conceptual model used in this report incorporates processes that describe subsurface flow and transport in a heterogeneous unsaturated zone. A discussion of these processes is provided in *Conceptual Model and Numerical Approaches for Unsaturated Flow and Transport* (BSC 2004 [DIRS 170035], Section 6). The software used in this study is iTOUGH2 V5.0 and T2R3D V1.4, which have been baselined through QA procedure IT-PRO-0011.

Acceptance Criterion 3—Data Uncertainty Is Characterized and Propagated through the Model Abstraction:

(1) Models use parameter values, assumed ranges, probability distributions, and bounding assumptions that are technically defensible, reasonably account for uncertainties and variabilities, and do not result in an under-representation of the risk estimate.

The parameter values were determined by model calibrations against site-specific field observations (Sections 6.2 and 6.3), and therefore are technically defensible and reasonably account for uncertainties and variabilities.

(4) The initial conditions, boundary conditions, and computational domain used in sensitivity analyses and/or similar analyses are consistent with available data. Parameter values are consistent with the initial and boundary conditions and the assumptions of the conceptual models for the Yucca Mountain site.

8. INPUTS AND REFERENCES

The following is a list of the references cited in this document. Column 2 represents the unique six-digit identifier (the Document Input Reference System number), which is placed in the text following the reference callout (e.g., BSC 2006 [DIRS 177465]). The purpose of these numbers is to assist in locating a specific reference. Within the reference list, multiple sources by the same author (e.g., BSC 2004) are sorted alphabetically by title.

8.1 DOCUMENTS CITED

Becker, M.W. and Shapiro, A.M. 2000. "Tracer Transport in Fractured Crystalline Rock: Evidence of Nondiffusive Breakthrough Tailing." W*ater Resources Research, 36*, (7), 1677-1686. Washington, D.C.: American Geophysical Union. TIC: 252313. 169947

BSC (Bechtel SAIC Company) 2001. *Pre-Test Predictions of Alcove 8 –Niche 3 Cross-Over Test.* Las Vegas, Nevada: Bechtel SAIC Company. ACC: MOL.20010904.0434. 155827

BSC 2004. *Conceptual Model and Numerical Approaches for Unsaturated Zone Flow and Transport.* MDL-NBS-HS-000005 REV 01. Las Vegas, Nevada: Bechtel SAIC Company. ACC: DOC.20040922.0006; DOC.20050307.0009. 170035

BSC 2004. *In Situ Field Testing of Processes*. ANL-NBS-HS-000005 REV 03. Las Vegas, Nevada: Bechtel SAIC Company. ACC: DOC.20041109.0001; DOC.20041109.0001; DOC.20051010.0001. 170004

BSC 2004. *Probability Distribution for Flowing Interval Spacing.* ANL-NBS-MD-000003 REV 01. Las Vegas, Nevada: Bechtel SAIC Company. ACC: DOC.20040923.0003. 170014

BSC 2004. *Saturated Zone In-Situ Testing.* ANL-NBS-HS-000039 REV 01. Las Vegas, Nevada: Bechtel SAIC Company. ACC: DOC.20041115.0008; DOC.20060116.0006. 170010

BSC 2004. *UZ Flow Models and Submodels.* MDL-NBS-HS-000006 REV 02. Las Vegas, Nevada: Bechtel SAIC Company. ACC: DOC.20041101.0004; DOC.20050629.0003. 169861

BSC 2005. *Q-List*. 000-30R-MGR0-00500-000-003. Las Vegas, Nevada: Bechtel SAIC Company. ACC: ENG.20050929.0008. 175539

BSC 2006. *Technical Work Plan for: Unsaturated Zone Flow, Drift Seepage and Unsaturated Zone Transport Modeling.* TWP-MGR-HS-000004 REV 04. Las Vegas, Nevada: Bechtel SAIC Company. ACC: DOC.20060824.0001. 177465

Zhou, Q.; Salve, R.; Liu, H.H.; Wang, J.S.Y.; and Hudson, D. 2006. "Analysis of a mesoscale infiltration and water seepage test in unsaturated fractured rock: Spatial variabilities and discrete fracture patterns." *Journal of Contaminant Hydrology, 87,* 96-122. New York, New York: Elsevier. Cataloging. 178226

LB0308A8N3TRTM.001. Seepage Travel Times in Niche 3 (9/4/02 - 3/29/03). Submittal date: 08/29/2003. 176448

LB0312A8N3MDLG.001. Pre-Test Prediction Results for Alcove 8/Niche 3: Simulations. Submittal date: 12/17/2003. 169761

LB0507A8N3SEEP.001. Niche 3 Seepage (3/26/2003-01/29/2004). Submittal date: 08/16/2005. 176445

LB0507A8N3SEEP.002. Niche 3 Seepage (01/29/2004-09/22/2004). Submittal date: 08/16/2005. 176446

LB0507A8N3SEEP.003. Niche 3 Seepage (9/22/2004-1/07/2005). Submittal date: 08/16/2005. 176447

MO0511UCC011JB.002. Fluoride, Bromide, Iodide, 2,6, Difluorobenzoic Acid (2,6 DFBA), 2,5, Difluorobenzoic Acid (2,5 DFBA), and 2,4,5 Trifluorobenzoic Acid (2,4,5 TFBA) Concentration Data for the Alcove 8/Niche 3 Tracer Test for Samples Collected 10/2003 through 12/2004. Submittal date: 11/04/2005. 176334

GS030108314224.001. Geotechnical Data for Alcove 8 (ECRB) and Niche 3 (ESF): Full Periphery Geologic Map (Drawing OA-46-356). Submittal date: 02/05/2003. 162131

8.4 SOFTWARE CODES

T2R3D V. 1.4. 1999. UNIX, Windows 95/98NT 4.0. STN: 10006-1.4-00. 146654

iTOUGH2 V. 5.0. 2002. SunOS 5.5.1, OSF1 V5.1, RedHat V7.2 and V7.3. STN: 10003-5.0-00. 160106

Two crosshole tracer tests involving the simultaneous injection of different tracers with different molecular diffusion coefficients were conducted in two different intervals at the C-wells complex near the Yucca Mountain site (Reimus et al. 2003 [DIRS 162950]). The test scale (the distance between injection and monitoring boreholes) is on the order of 30 m. Details of the tests can be found in the study by Reimus et al. (2003 [DIRS 162950]).

By fitting tracer breakthrough curves observed at the monitoring borehole, Reimus et al. (2003 [DIRS 162950]) estimated values of flow and transport parameters for the test site. They include parameter A:

$$A = \frac{\phi_m}{b}\sqrt{D_m} \qquad \text{(Eq. A-1)}$$

where b is the half fracture aperture, ϕ_m is the matrix porosity, and D_m is the effective matrix diffusion coefficient. For the given values for field-scale A_F and ϕ_m and based on Equation A-1, one can have:

$$F_d = \frac{D_{m,F}}{D_{m,L}} = \frac{\left(\frac{A_F b_F}{\phi_m}\right)^2}{D_{m,L}} = \frac{{b_F}^2}{(\frac{\phi_m\sqrt{D_{m,L}}}{A_F})^2} = \left(\frac{b_F}{b*}\right)^2 \qquad \text{(Eq. A-2)}$$

where F_d is the ratio of the field-observed effective matrix diffusion coefficient ($D_{m,F}$) to the corresponding value obtained from rock matrix samples at the lab ($D_{m,L}$). The subscripts F and L correspond to field and lab scales, respectively. The b_F and b* are calculated based on $D_{m,F}$ and $D_{m,L}$, respectively, for the given field-scale A_F and ϕ_m and other flow and transport parameters. (The parameter b* is not a lab-scale fracture aperture.) The upper bound values for 2b* are 1.06 cm for the Prow Pass geological unit and 1.28 cm for the Bullfrog unit (Reimus et al. 2003 [DIRS 162950], Table 6). (Note that the use of the upper bound values is to avoid overestimating F_d values.) The tests were performed for the two geological units.

Assuming the conductive horizontal fractures to be represented by two perpendicular sets of identical parallel infinite fractures with a fracture spacing L, one can approximate the flow porosity ε by:

$$\varepsilon = \frac{4b_F}{L} \qquad \text{(Eq. A-3)}$$

By analyzing flow and tracer transport data, Reimus et al. (2003 [DIRS 162950], Table 6) obtained ε = 0.003 for both geological units when radial flow test conditions were assumed. While parameter values are also available for the assumed linear flow test condition (Reimus et al. 2003 [DIRS 162950]), it is believed that radial flow more appropriately represents the actual test conditions for the given test configuration.

The probability distribution for flow interval spacing in the saturated zone of Yucca Mountain was discussed and documented in *Probability Distribution for Flowing Interval Spacing* (BSC 2004 [DIRS 170014]). The geometric mean flow interval spacing is $10^{1.29}$ m = 19.50 m (BSC 2004 [DIRS 170014], Table 6-7). Considering the mean flow interval spacing to be the same as the average value for L, one can use Equation A-3 to estimate b_F and further use Equation A-2 to estimate F_d. The estimated values for F_d are 8 and 5 for the Prow Pass and Bullfrog units, respectively. F_d values larger than one indicate the enhancement of the effective matrix diffusion coefficient discussed in Section 6.4.

Note that a number of assumptions or simplifications were used to estimate b_F (and therefore F_d) in the above discussion, which may involve a relatively large degree of uncertainty. The mass transfer parameter A_F is estimated directly from the tracer breakthrough curves, but the underlying parameters ϕ_m, b_F, and $D_{m,F}$ cannot be uniquely and independently estimated from the tracer testing results alone. These parameter values could also be estimated from other measurements combined with the tracer test results. For example, ϕ_m and $D_{m,L}$ can be estimated from laboratory core measurements (these estimates were used to obtain the estimate of b^* given the value of A_F determined from C-wells tracer testing), and b_F can be estimated from flow porosity estimates assuming a given flow path geometry. There is generally a small degree of uncertainty in the parameter ϕ_m for a given rock unit, but estimates of b_F (and hence the calculated value of $D_{m,F}$ for a given value of A_F) involve significant uncertainty because of the uncertainties in flowing interval measurements and in the assumption that a flowing interval consists of one large-aperture fracture. However, the best available information from the test analysis results and other sources has been used in estimating F_d here. Also note that the estimated fracture aperture from Equation A-3 is 2.93 cm, which is considerably larger than expected for a single fracture. This can be explained by the notion that a flow path consists of a group of fractures, rather than a single fracture. This issue was further discussed in Section 6.4.1.

Note that the analyses from this appendix are not inconsistent with the results discussed in *Saturated Zone In-Situ Testing* (BSC 2004 [DIRS 170010], Section E 4.2). The study in that report (BSC 2004 [DIRS 170010], Section E4.2) focuses on parameter A (Equation A-1) and showed that values for lab-scale A are larger than the corresponding field-scale values. This is because rock samples used for the lab tests generally contain much smaller fractures than those important for field-scale tracer transport as a result of sample collection procedures and the scarcity of conductive fractures associated with flow channels in the field. In this case, a larger field aperture gives a smaller A value. This, however, does not necessarily suggest that field-scale matrix diffusion coefficient is smaller than the lab-scale value, but indicates that changes in apertures have a large effect on A values. This analysis also shows that if saturated zone transport models assume the expected value of the flowing interval spacing, L, and a value of b that is calculated from Equation A-3 (using L and the flow porosity inferred from tracer testing; i.e., b_F) as the "true" large-scale field values of these parameters, then the laboratory-measured matrix diffusion coefficient, $D_{m,L}$, must be multiplied by a factor of b_F^2/b^{*2} (in this case, 5 to 8) to obtain an effective matrix diffusion coefficient $D_{m,F}$ that will yield a large-scale A value that is equal to the A value determined in the C-wells tests. However, it is uncertain how representative the A values determined in the C-wells tests are for much larger scales.